Aero-hydro-elastic simulation of a semi-submersible floating wind turbine

Maxime Philippe, Aurélien Babarit, Pierre Ferrant

▶ **To cite this version:**

Maxime Philippe, Aurélien Babarit, Pierre Ferrant. Aero-hydro-elastic simulation of a semi-submersible floating wind turbine. ASME 2012 International Conference on Ocean, Offshore and Artic Engineering (OMAE2012), Jul 2012, Rio de Janeiro, Brazil. 10.1115/OMAE2012-84070 . hal-01202076

HAL Id: hal-01202076
https://hal.science/hal-01202076

Submitted on 25 Apr 2019

HAL is a multi-disciplinary open access archive for the deposit and dissemination of scientific research documents, whether they are published or not. The documents may come from teaching and research institutions in France or abroad, or from public or private research centers.

L'archive ouverte pluridisciplinaire **HAL**, est destinée au dépôt et à la diffusion de documents scientifiques de niveau recherche, publiés ou non, émanant des établissements d'enseignement et de recherche français ou étrangers, des laboratoires publics ou privés.

Proceedings of the ASME 2012 31st International Conference on Ocean, Offshore and Arctic Engineering
OMAE2012
July 1-6, 2012, Rio de Janeiro, Brazil

OMAE2012-84070

AERO-HYDRO-ELASTIC SIMULATION OF A SEMI-SUBMERSIBLE FLOATING WIND TURBINE

Maxime PHILIPPE*
Aurélien BABARIT
Pierre FERRANT
LHEEA Lab. (ECN-CNRS)
École Centrale Nantes, LUNAM Université
Nantes, 44321
France
Email: maxime.philippe@ec-nantes.fr

ABSTRACT

This paper presents an aero-hydro-elastic model of a semi-submersible floating wind turbine. A specific attention is drawn to hydrodynamic modelling options and its effect on the dynamic response of the platform.

The NREL 5MW reference wind turbine mounted on the historical concept of semi-submersible platform Dutch Tri-floater is considered. A specific hydrodynamic model of loads on semi-submersible platform is used within the wind turbine design code FAST from NREL. This hydrodynamic model includes non linear hydrostatic and Froude-Krylov forces, diffraction/radiation forces obtained from linear potential theory, and Morison forces to take into account viscous effects on the braces and damping plates. The effect of the different hydrodynamic modelling options is investigated. As one could have expected, it is found that the effect of viscous drag and non linear Froude-Krylov loads, becomes larger with increasing wave height. Simulations are run with directional wave spectrum, it is found that wave directionality induces larger transverse motions.

INTRODUCTION

Numerous floating wind turbine concepts are currently being studied; they are mostly based on offshore O&G technology. Among them, semi-submersible platforms are gaining recent industrial attention [1]. For this type of platform, wave loads will be significant due to the large floating area, and could induce relatively large motions of the structure. Therefore, minimizing wave loads action on the structure will be in the center of the conception process [2].

Numerical simulations of floating wind turbine response should take into account aerodynamic loading and damping, hydrodynamic loading damping, and gyroscopic effect. Several numerical models have been developed to combine these effects in a coupled simulation. Some of them resolve the motions in frequency domain [3]; in that case hydrodynamic loads are calculated with linear potential flow theory. In the case of time domain simulations, linear potential theory can also be used to calculate hydrodynamic loads [4]. It allows to take into account for linear hydrodynamic radiation and linear diffraction loads. This linear approach is valid in the case of small motions regarding to body length. Another approach is to use Morison equation to calculate the hydrodynamic loads [5]. But the Morison equation is only relevant in the case of slender body. A combination of linear potential theory forces and viscous drag forces can be used to model these different effects as done for instance by [6, 7], second order potential forces may also be taken into account [8]. The linear hydrodynamic theory is valid only when linearisation assumptions are respected. When these hypotheses are not respected it

*Address all correspondence to this author.

is possible to add some non linear formulations for certain loads, as viscous drag. This combination of linear loads and non linear loads is not consistent with linearisation process, but it has been found that it improves the results in practice. This approach is commonly used in offshore O&G industry, in particular for semi-submersible platforms.

This study aims at evaluating the effect of hydrodynamic modelling options on the results of aero-hydro-elastic simulations of semi-submersible floating wind turbine. A focus has been placed on the effect of viscous drag, on the effect of non linear Froude-Krylov loads (calculated on instantaneous wetted surface), and on the effect of wave directionality.

FAST design code [9] from National Renewable Energy Laboratory (NREL) is used to model the NREL 5MW reference wind turbine, which is mounted on the historical concept of semi-submersible platform Dutch Tri-floater [10]. A specific hydrodynamic model of loads on semi-submersible platform has been developed for FAST. It is based on the use of diffraction/radiation theory, Morison loads, and non-linear hydrostatic and Froude-Krylov loads. The effect of hydrodynamic modelling on the motions of the structure is investigated. This model is used to compute the motions of the system in regular waves, with and without viscous drag, and with and without non linear Froude-Krylov loads, in order to assess their effects. These effects are studied with regards to the wave height. Motions of the floating wind turbine in irregular waves are also computed. In particular the effect of a directional wave spectrum, on the motions of the whole system and on the power production, is investigated.

MODEL DEVELOPMENT

Aero-hydro-elastic simulations are run with FAST design code from NREL [9]. FAST includes a platform load model named HydroDyn [6]; this model has not been used in the present study. Instead, a user-defined model for the hydrodynamic loads on the platform has been developed to allow us to model non linear Froude-Krylov loads and viscous drag on the braces.

Incident wave modelling

In this paper incident wave is modelled according to linear theory in infinite water depth, as the sum of a large number of Airy waves. Free surface elevation η is computed as follow (eq. 1) :

$$\eta(x,y,t) = \sum_{i=1}^{N_\beta} \sum_{j=1}^{N_\omega} A(\omega_i,\beta_i) sin\left[k_i(xsin\beta_j + ysin\beta_j) - \omega_i t + \phi_{ij}\right] \tag{1}$$

where : $A_i^2 = 2S(\omega_i,\beta_i)\delta_{\omega_i}\delta_{\beta_i}$ with $S(\omega,\beta)$ is the directional wave spectrum, ϕ_{ij} represents the phase uniformly distributed as an independent stochastic variable.

The directional wave spectrum $S(\omega,\beta)$ is simply defined as $S(\omega,\beta) = S(\omega)G(\beta)$. With $S(\omega)$ is the frequency wave spectrum. In our platform model the JONSWAP spectrum is used. $G(\beta)$ is the direction spreading function. $G(\beta)$ is defined classically as defined by [11] :

$$G(\beta) = C_1(s)cos^{2s}\frac{\beta - \overline{\beta}}{2} ; \pi \geq \beta - \overline{\beta} \leq \pi \tag{2}$$

with $\overline{\beta}$ the mean wave direction. $C_1(s)$ is a normalization coefficient. A value of s=10 represents wind wave, s=25 is suitable for small wavelength waves, and s=75 is suitable for long waves [12]. An example of directional wave spectrum is plotted on figure 1 for s=40.

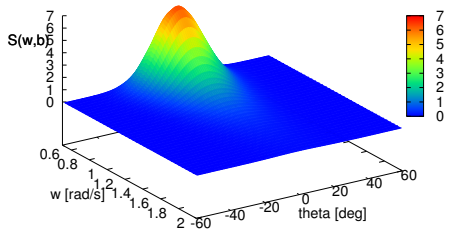

FIGURE 1: Directional wave spectrum for γ=1 (Pierson-Moskowitz) and s=40

Platform load modelling

FAST solves the equation of motion of the wind turbine system in time domain. This equation can be written as eq. (3).

$$M_{sys}\ddot{X} = F + F_{ptfm} \tag{3}$$

In this equation F_{ptfm} is the vector of the loads on the platform and F is the vector for other loads. In this study the focus is on the calculation of F_{ptfm} vector. Loads on the platform F_{ptfm} are calculated, according to eq. (4), as the sum of the following contribution :

radiation loads F_{rad},
diffraction loads F_{dif},
Froude-Krylov loads F_{FK},
hydrostatic loads F_{hstc},
a contribution from Morison equation F_{mori},
mooring loads F_{anc}.

Calculation of the different terms is detailed below.

$$F_{ptfm} = F_{rad} + F_{dif} + F_{FK} + F_{hstc} + F_{mori} + F_{anc} \quad (4)$$

Radiation loads are calculated according to linear potential flow theory (eq. 5). $\mu_{\infty,ij}$ is the added mass matrix, and K_{ij}^{rad} is the matrix of the memory terms of the radiation force. These matrices can be calculated with a diffraction/radiation code such as WAMIT.

$$F_j^{rad} = -\mu_{\infty,ij}\ddot{X}_j - \int_0^t K_{ij}^{rad}(t-\tau)\dot{X}_j(\tau)d\tau \quad (5)$$

Diffraction loads F_{dif} are also calculated with linear hydrodynamic theory, using diffraction impulse responses K_7, according to eq. (6). $\eta_0^{\beta_i}$ is the wave elevation associated to the incident wave direction β_i.

$$F_{dif}(t) = \sum_{i=1}^{N_\beta} \int_{-\infty}^{+\infty} K_7(t-\tau,\beta_i)\eta_0^{\beta_i}(t)d\tau \quad (6)$$

Froude-Krylov loads F_{FK} can be calculated on the mean free surface according to linear theory (eq. 7). Alternatively, these loads may also be calculated on the instantaneous wetted surface according to eq. (8). These loads are named non linear Froude-Krylov when they are integrated on the instantaneous wetted surface. Contribution of these loads in non linear behaviour of vessels has been studied in [13], and comparisons of numerical simulations and experiments for large amplitude motions of wave energy converters have shown satisfying agreement [14].

$$F_{FK}(t) = \sum_{i=1}^{N_\beta} \int_{-\infty}^{+\infty} K_{ex}(t-\tau,\beta_i)\eta_0^{\beta_i}(t)d\tau \quad (7)$$

$$f^{FK} = -\int_S p_d \vec{N} dS \quad (8)$$

where p_d is the dynamic pressure force associated with incident wave potential, such as $p_d = -\rho\frac{\partial\phi_i}{\partial t}$. ϕ_i is the 1st order potential associated with incident wave, and S is the instantaneous wetted surface. $\vec{N}$ is the generalized normal vector.

Hydrostatic loads can also be calculated either on the mean free surface (eq. 9) or on the instantaneous wetted surface (eq. 10).

$$f^{hstc} = -K_h X \quad (9)$$

K_h is the hydrostatic stiffness matrix as defined in [4].

$$f^{hstc} = -\int_S p_s \vec{N} dS \quad (10)$$

p_s is the static pressure such as $p_s = p_0 - \rho g z$.

Morison loads permit to take into account some loads which are not modelled in the previous terms, namely drag loads. Morison equation gives the loads on a cylindrical body placed in an oscillatory flow [15]. For a slice of cylinder located in (X(t),Y(t)) and for a flow (U(t),V(t)) in the plane of the slice, Morison loads can be written as eq. (11).

$$\begin{pmatrix} dF_X \\ dF_Y \end{pmatrix} = \underbrace{\frac{1}{2}\rho C_D \begin{pmatrix} U-\dot{X} \\ V-\dot{Y} \end{pmatrix} \sqrt{(U-\dot{X})^2+(V-\dot{Y})^2}\, dL}_{I} + \underbrace{\left[\rho(1+C_m)\pi\frac{D^2}{4}\begin{pmatrix} \dot{U} \\ \dot{V} \end{pmatrix} \underbrace{-\rho C_m \pi \frac{D^2}{4}\begin{pmatrix} \ddot{X} \\ \ddot{Y} \end{pmatrix}}_{III} dL \right]}_{II} \quad (11)$$

In eq. (11), term 1 represents the drag loads and term 2 represents the inertia loads. C_D and C_m coefficients can be determined experimentally. To calculate the Morison loads on the floater, the structure is partitioned into elements of cylinder. The total load is integrated along the cylinders composing the structure. Inertia loads are only calculated for the elements of the structure which are not modelled with potential theory or direct pressure integration. Drag loads are calculated for the small diameter elements.

Mooring loads F_{anc} are calculated with an equivalent linear stiffness matrix and a constant vertical pretension, $F_{anc} = F_{a,0} - K_a X$.

MODEL PROPERTIES

Floating wind turbine properties

The floating platform used in this study is the historical concept known as the Dutch Tri-floater. It is a column stabilized platform composed of 3 columns of 8 m diameter separated by 68 m. These 3 columns are connected with braces which also support the wind turbine. Heave plates are placed at the bottom of each column in order to reduce amplitude of motions. Table 1 summarizes some properties of the floater. All properties can be found in [10].

The wind turbine mounted on this platform is the reference 5 MW turbine from NREL [16]. This wind turbine is designed to have a hub height of 90 m. The tower of the turbine has been adapted in order to fit this value and to connect with the Dutch Tri-floater. The length of the new tower is 62.6 m, the base diameter is 8m and the mass is 328 t.

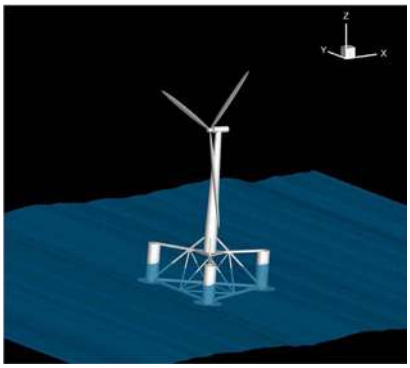

FIGURE 2: Representation of the system

Floater mass	1148,0 te
Ballast mass	435,2 te
Turbine mass	678,3 te
Mooring pretension	183,5 te
System center of mass	19,0 m
Buoyancy center	-7,1 m
Displacement	2545,0 te

TABLE 1: Summary of system properties

Hydrodynamic loads calculation

The Dutch Tri-floater platform is composed of different parts:

the 3 columns,
the braces,
the 3 heave plates.

Each of these parts have different dimensions and therefore should be considered differently for the hydrodynamic load calculation.

As the dimension of the 3 columns is relatively large, linear potential theory is adapted to compute the hydrodynamic loads exerted on it. This theory is used in the present study. For the braces, as the diameters are relatively small, wave damping will be negligible compared to viscous drag. Order of magnitude of Keulegan-Karpenter number K_C is 3 to 7 for 1m waves. Therefore Morison drag will be applied to the braces. Inertial loads can be calculated with linear potential theory for the braces. So they are not taken into account in the Morison calculation, but they are taken into account in the potential flow calculation.

Figure 3c represents the mesh used for the calculation of linear hydrodynamic properties (added mass, wave damping and excitation force). This calculation has been performed with Aquaplus [17]; the floater has been considered in steady state position (position due to a constant wind and without waves). The mesh used for the calculation of non linear Froude-Krylov loads is represented on figure 3d. Figure 3b shows the mesh used for the calculation of Morison viscous drag on the braces. A viscous drag coefficient C_d of 0.7 was chosen.

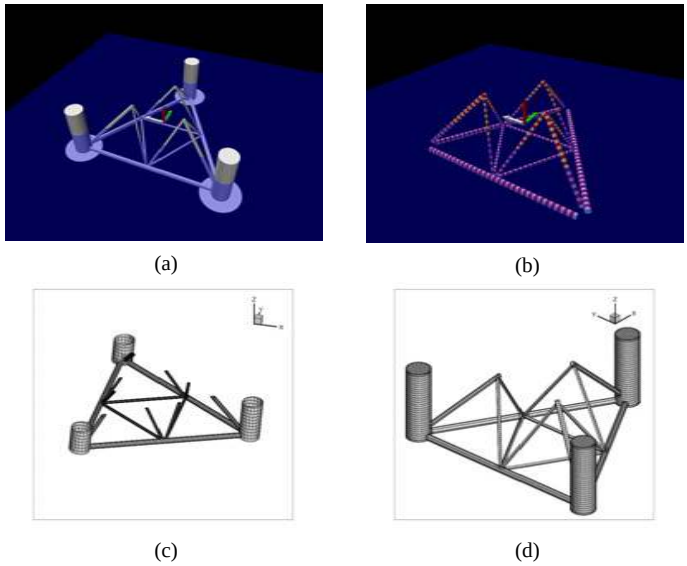

FIGURE 3: 3a: view of the platform - 3b: Mesh of the braces for Morison drag loads calculation - 3c: Mesh of Dutch Tri-floater platform used with Aquaplus for potential flow calculation - 3d: Mesh used for non linear Froude-Krylov loads calculation

Heave plates of the platform have a diameter of 18 m. Such heave plates have been used by O&G industry, in particular for spar platforms. They are thought to reduce the platform motions. These plates have 2 simultaneous effects :

they create viscous damping due to flow separation at edges,
they increase the heave added mass; it may shift the natural periods out of wave range period.

In case of a semi-submersible platform, draft is reduced, and the plates are located near the free surface (with comparison to a spar). In that case the plates also increase wave excitation forces [18]. This effect is balanced by the increase of damping. The main effect remains the shift of natural frequency. Ishiara et al. [19] studied the influence of heave plates in the case of semi-submersible floating wind turbine through water tank test. They found that these plates increase heave natural period and reduce motions at extreme sea states.

In this paper the effect of the plates on the platform motions is modelled with an in line (in plate axis) Morison force. Drag and inertia coefficients C_d and C_m have to be determined for the geometry of the plates. According to Bearman et al. [20], drag coefficient for a rectangular planar plate is $7.8K_C^{1/3}$ (with K_C the Keulegan Carpenter number). It gives an order of 6 - 10 for our geometry; a C_d value of 8 has been chosen. Regarding the added mass coefficient C_m, the added mass of an oscillating cylindrical plate is the mass of the equivalent hemisphere [21]. In the case of a plate and a cylinder, the contribution of cylinder is deducted and added mass becomes eq. (12) [22].

$$m_a = \frac{1}{3}\rho D_d^3 - \left[\frac{\pi\rho}{8}D_c^2(D_d - \sqrt{D_d^2 - D_c^2}) + \frac{\pi\rho}{24}\left(D_d - \sqrt{D_d^2 - D_c^2}\right)^2\left(2D_d + \sqrt{D_d^2 - D_c^2}\right)\right] \quad (12)$$

with D_c the diameter of the cylinder and D_d the diameter of the plate. Eq. (12) has been used to calculate the added mass value used in the Morison equation.

Mooring loads modelling

Mooring loads are calculated as a linear restoring force and a constant vertical load. The stiffness matrix is calculated with OrcaFlex [23]. The same mooring system as the one proposed in [10] has been used. This is a 6 lines mooring system, each line is composed of 190 m of cable and 225 m of chain (chain length is slightly reduced by comparison to [10]). Figure 4 shows a picture of mooring system modelling. By perturbing each platform degree of freedom (DOF), the stiffness matrix has been calculated, and the following representation for the mooring system has been obtained:

$$F_a = F_{a,0} - K_a X \quad (13)$$

$$F_{a,0} = \begin{pmatrix} 0 \\ 0 \\ -1.8\cdot 10^5 \\ 0 \\ 0 \\ 0 \end{pmatrix} \quad (14)$$

$$K_a = \begin{pmatrix} 1.6\cdot 10^5 & 0 & 0 & 0 & 1.9\cdot 10^6 & 0 \\ 0 & 1.6\cdot 10^5 & 0 & -1.9\cdot 10^6 & 0 & 0 \\ 0 & 0 & 1.5\cdot 10^5 & 0 & 0 & 0 \\ 0 & -1.9\cdot 10^6 & 0 & 1.1\cdot 10^8 & 0 & 0 \\ 1.9\cdot 10^6 & 0 & 0 & 0 & 1.1\cdot 10^8 & 0 \\ 0 & 0 & 0 & 0 & 0 & 1.7\cdot 10^8 \end{pmatrix} \quad (15)$$

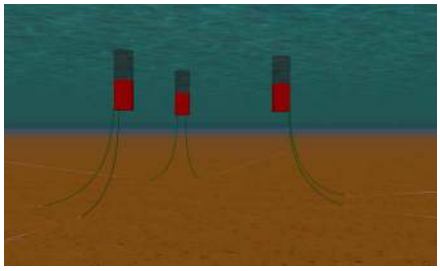

FIGURE 4: Picture of the mooring system modelling with OrcaFlex [23]

RESULTS

Properties of the 4 models compared

In this paper the results of the 4 following platform load models are compared:

M1 is the most complete model. Radiation and diffraction loads are calculated with linear theory. Hydrostatic and Froude-Krylov loads are calculated on instantaneous wetted surface. Drag loads of the Morison equation are also included.

M2 is the same as M1 except that hydrostatic and Froude-Krylov loads are calculated with linear theory.

M3 is the same as M1 except that Morison loads are not taken into account.

M4 is the simplest model. Radiation, diffraction, Froude-Krylov and hydrostatic loads are calculated according linear theory, and viscous drag is not calculated. The only non linear hydrodynamic terms come from the damping plate modelling.

Properties of these 4 models are summarized in table 2 below.

Simulation cases description

Time domain simulations with the 4 models M1, M2, M3 and M4 have been run. For all simulations presented here, the water depth is considered as infinite; wind and wave are supposed to be aligned; wind speed is constant at 11.2 m/s; the wind turbine model is a FAST fully flexible model. Three different types of simulation have been run :

	Radiation	Diffraction	Froude Krylov	Hydrostatic	Morison drag on braces
M1	Lin	Lin	NL	NL	Cd=0.7
M2	Lin	Lin	Lin	Lin	Cd=0.7
M3	Lin	Lin	NL	NL	no
M4	Lin	Lin	Lin	Lin	no

TABLE 2: Properties of the 4 hydrodynamic load models (Lin: linear, NL: non linear)

First simulations, E1, are time series of 2000s. Wave amplitude is 1m and wave frequency varies from 0.05 to 2.05 rad/s ; waves are regular. The system reaches a permanent state after a transient state. "Effective Response Amplitude Operators" (RAO) are deduced from the permanent oscillations around a mean position. The results obtained with the 4 platform loads models M1, M2, M3 and M4 are compared. Second kind of simulations E2 are also ran with regular waves. 2 wave frequency 0.6 rad/s and 1 rad/s have been chosen, and varied the wave amplitude from 0.1 m to 6 m, to identify the influence of wave height. Again the results for the 4 platform models are compared.
Finally irregular waves simulations have been run with platform model M4. Incident waves characteristics are Hs=6m, Tp=10s with a Pierson Moskovitz spectrum. The results of uni-directional wave are compared with the results for directional wave with a spreading parameter s=40.

Characteristics of these simulations are summarized in table 3

Effect of non linear Froude-Krylov loads and viscous drag

Effective Response Amplitude Operators. Results of E1 simulations are shown on figures 5 and 6. Figure 5 shows the RAOs of the platform surge, heave, pitch and yaw motions. For the surge motion, the results of the 4 models are in good agreement, except around the resonant response around 0.2 rad/s. Around 0.2 rad/s, non linear Froude-Krylov loads slightly increase the response, the difference is not large. For pitch motion, the differences between models are also small. Model M1 and M3 (with non linear Froude-Krylov) give the largest motion around 0.6 rad/s.

For yaw motion the effect of non linear Froude-Krylov is noticeable for low frequency. But the order of magnitude of yaw remains small in all simulations, The permanent state for transverse motions is not perfectly reached, so is is difficult to conclude on this effect.

Figure 6 represents the RAOs of tower top deflection and out of plane tip deflection. As the difference between hydrodynamic model were not large for platform motion, the differences in wind

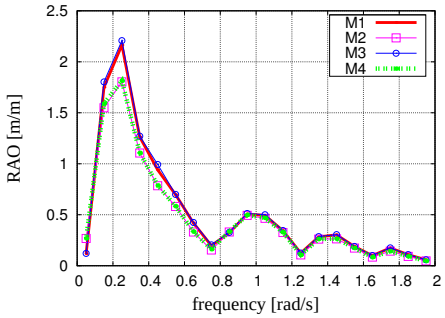

(a) surge

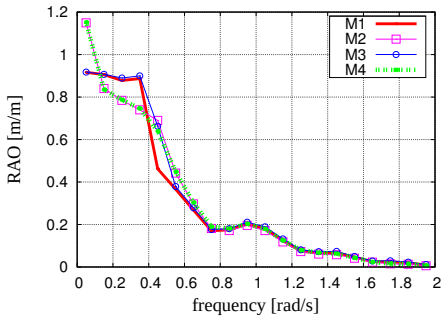

(b) heave

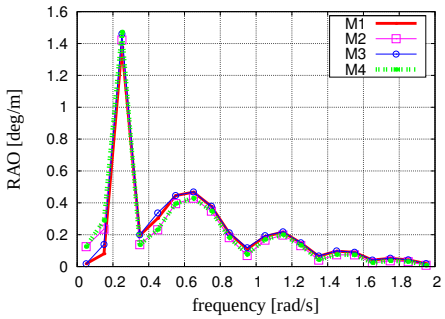

(c) pitch

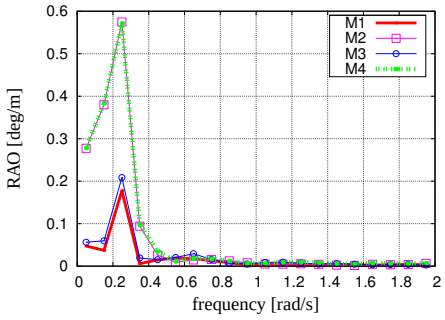

(d) yaw

FIGURE 5: Effective RAOs of the platform surge, heave, pitch and yaw motions

	Description	Wave conditions	Models used
E1	Time-series-generated "effective RAOs"	Regular Airy - A=1m ω =0.05, 0.015, ... 2.05 rad/s	M1,M2,M3,M4
E2_1	Periodic time series - Effect of wave amplitude	Regular Airy - A=0.1m ... 6m - ω =0.6 rad/s	M1,M2,M3,M4
E2_2	Periodic time series - Effect of wave amplitude	Regular Airy - A=0.1m ... 6m - ω =1.0 rad/s	M1,M2,M3,M4
E3_1	Time series statistics, Power spectra - Effect of wave directionality	Irregular Airy - γ =1- Hs=6m - Tp=10s	M1
E3_2	Time series statistics, Power spectra - Effect of wave directionality	Irregular directional Airy - γ =1 - s=40 - Hs=6m - Tp=10s	M1

TABLE 3: Simulation cases specifications

turbine motion are also small. The larger yaw observed on figure 5d has no effect on blade motion, probably because yaw motion remains small.

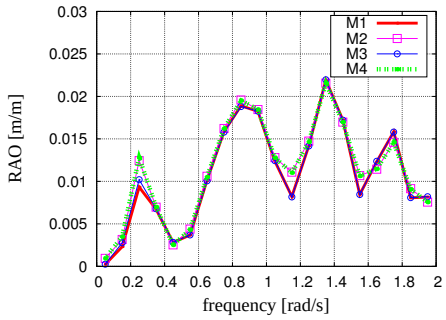

(a) tower top deflection

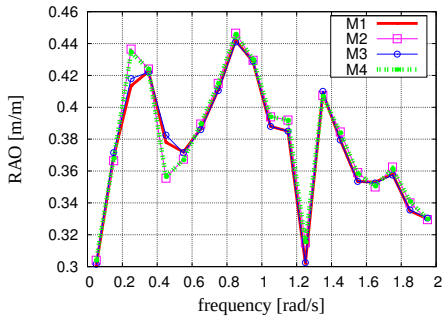

(b) out of plane blade tip deflection

FIGURE 6: Effective RAOs of the tower top deflection and out of plane blade tip deflection,

Wave height sensitivity. For 1 m amplitude incident wave, results between the 4 models were not very different. For 0.6 rad/s and 1 rad/s waves, the influence of wave height has been studied. Figure 7 represents the results for pitch and tower top deflection, in the case of 1 rad/s incident wave. The differences between the models become more significant when wave height increases, but orders of magnitude remain the same. For model M3 and M4 (without Morison drag), there is no result plotted for 6 m amplitude because the simulations became unstable without Morison drag.

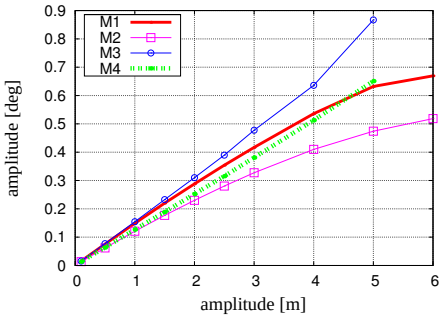

(a) pitch

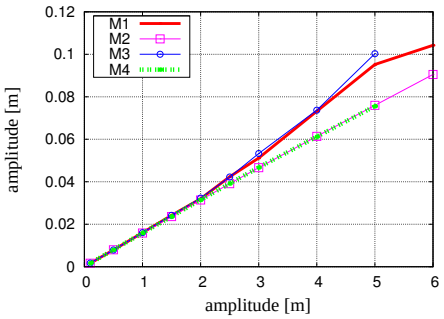

(b) tower top deflection

FIGURE 7: Amplitude of pitch motion and tower top deflection around a mean position with regards to wave amplitude for an incident wave of pulsation $\omega = 1 rad.s^{-1}$

For 0.6 rad/s incident wave, results are shown on figure 8. For model M4, the simulations were not stable for amplitude greater than 3m, that is why there are no results plotted. Same conclusions are obtained as for 1 rad/s waves, the differences between models become larger with increasing wave height, but orders of magnitude remain the same.

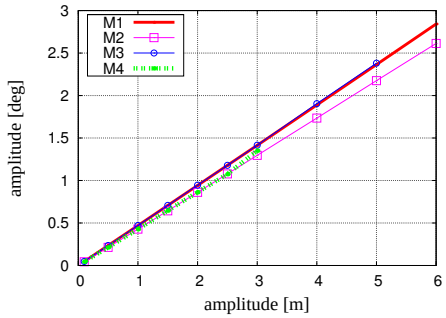

(a) pitch

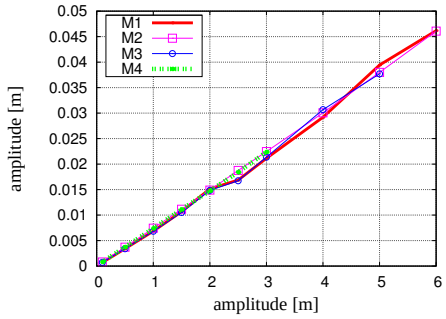

(b) tower top deflection

FIGURE 8: Amplitude of pitch motion and tower top deflection around a mean position with regards to wave amplitude for an incident wave of pulsation $\omega = 0.6 rad.s^{-1}$

Influence of wave directionality

Results of simulations with irregular unidirectional waves (E3-1) and simulations with irregular directional waves have been compared. Simulations run-time is 600 s. On these 600 s the 300 first are not taken into account for statistics in order to avoid transient computational effects. It remains 300 s for the statistics. Wave elevation for these 300 seconds is shown on figure 9 for the two simulations. One should note the duration of simulation is short (5 min) for the statistics, and the 300 s of simulation before statistics may be not enough to ensure a permanent state, in particular for the transverse motions. Nevertheless, the trends observed seem significant.

An increase of transverse motions (sway, roll and yaw) of the platform is observed. Comparison of yaw motions has been plotted on figure 10b. This increase of yaw motion could lead to an increase of structural loads, which should be taken into account for design. Regarding axial motions (surge, heave, pitch), a reduction of amplitude is observed (see figure 10a for the representation of pitch motion). Statistics for surge, pitch and yaw motions are presented in table 4.

Concerning the generated power, wave directionality seems to have little influence on mean generated power and standard deviation. Table 4 presents these statistics and figure 11 shows

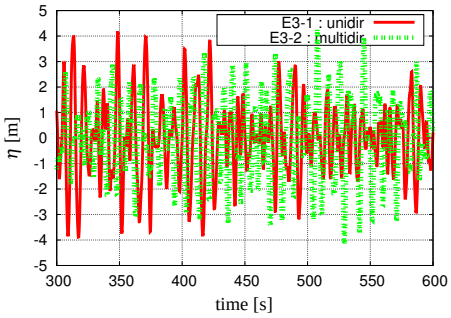

FIGURE 9: Wave elevation for irregular directional waves and uni-directional waves

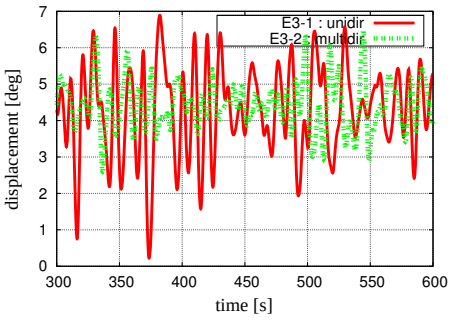

(a) pitch

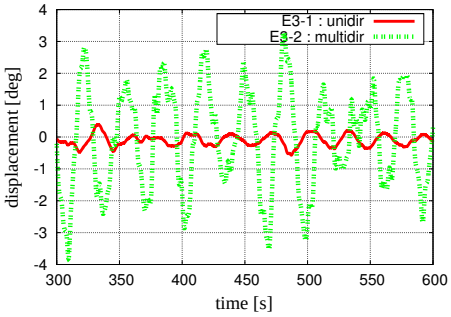

(b) yaw

FIGURE 10: Comparison of pitch an yaw motions in irregular directional waves and uni-directional waves

the power spectral density of the generated power obtained for the two simulations. Regarding the tower top fore-aft deflection a relative reduction of amplitude is noted. This reduction is probably due to the reduction of axial motion of the platform. Concerning the blades out of plane deflection, no significant influence is observed. Statistics for these displacements are presented in table 4. Figure 12 shows the power spectral density of the tower fore-aft deflection.

	GenPwr [kw]		TTDspFA [m]		OOPDelf1 [m]	
	Mean	StdDev	Mean	StdDev	Mean	StdDev
E3-1 : Unidir	4664,2	388,7	0,10	0,04	5,45	0,36
E3-2 : Multidir	4668,0	342,5	0,10	0,02	5,48	0,30

	Surge [m]		Pitch [deg]		Yaw [deg]	
	Mean	StdDev	Mean	StdDev	Mean	StdDev
E3-1 : Unidir	3,67	1,20	4,28	1,23	-0,10	0,18
E3-2 : Multidir	3,58	0,99	4,43	0,68	-0,10	1,60

TABLE 4: Statistics for generated power, tower deflection, blade deflection, surge, pitch and yaw, in case of irregular directional waves and uni-directional waves

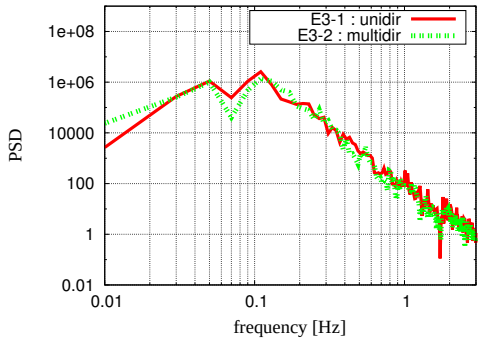

FIGURE 11: Power spectral density of generated power, in case of irregular directional waves and uni-directional waves

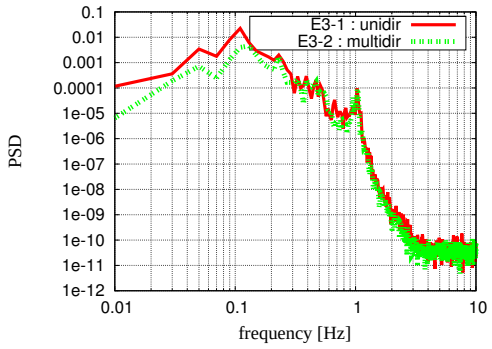

FIGURE 12: Tower fore-aft deflection power spectral density, in case of irregular directional waves and uni-directional waves

CONCLUSION

In this paper the results of time domain simulations of a semi-submersible floating wind turbine have been compared for 4 different models of hydrodynamic loads on the floater. Then the effect of wave directionality on the system in irregular waves has been studied.

The 4 platform load models gave similar results for small amplitude waves. Viscous drag and non linear Froude-Krylov have little influence for small waves.

With increasing wave height, the differences become larger. Non linear Froude-Krylov loads and Morison drag permit to simulate larger motion without instabilities. In some cases, the most complete model (with Morison drag and non linear Froude-Krylov loads) brings out the larger motions, however order of magnitude remains the same. It highlights the importance of taking into account non linear hydrodynamic loads for the simulation of large motions of floating wind turbine. These results have to be confirmed with wave tank test.

Concerning the effect of wave directionality, an increase of transverse motions, sway, roll, yaw, and a reduction of axial, surge, pitch and yaw motions, have been observed. No significant influence on the generated power has been observed.

In the present study extreme waves have not been considered. In the case of extreme conditions, floater dimensions become small regarding to wave amplitude. The use of Morison equation could be considered to calculate the hydrodynamic loads on the entire floater. Further investigations are needed to see the influence of hydrodynamic modelling of semi-submersible floating wind turbine in case of extreme waves.

ACKNOWLEDGMENT

The authors would like to acknowledge ADEME (the French environment agency) and Région Pays de la Loire for funding the Phd program in which this study has been done.

REFERENCES

[1] Roddier, D., Peiffer, A., Aubault, A., and Weinstein, J., 2011. "A generic 5mw windfloat for numerical tool validation and comparison against generic spar". International Conference on Ocean, Offshore and Arctic Engineering.

[2] Henderson, A., and Witcher, D., 2010. "Floating offshore wind energy-a review of the current status and an assessment of the prospects". *Wind Engineering*, ***34***(1), pp. 1–16.

[3] Wayman, E., Sclavounos, P., Butterfield, S., Jonkman, J., and Musial, W. "Coupled dynamic modeling of floating wind turbine systems". In 2006 Offshore Technology Conference, 1–4 May 2006, Houston, TX.

[4] Jonkman, J., 2007. "Dynamics Modelling and Load Anal-

ysis of an Offshore Floating Wind Turbine". PhD Thesis, University of Colorado.

[5] Whithee, J., 2004. "Fully coupled dynamic analysis of a floating wind turbine system". PhD Thesis, Department of Ocean Engineering, MIT.

[6] Jonkman, J., 2009. "Dynamics of offshore floating wind turbines - model development and verification". *Wind Energy,* ***12***, pp. 459–492.

[7] Cermelli, C., Roddier, D., and Aubault, A., 2009. "Windfloat: a floating foundation for offshore wind turbines part ii: Hydrodynamic analysis". International Conference on Ocean, Offshore and Arctic Engineering.

[8] Ormberg, H., Passano, E., and Luxcey, N., 2011. "Global analysis of a floating wind turbine using an aero-hydroelastic model: Part 1code development and case study". International Conference on Ocean, Offshore and Arctic Engineering.

[9] J. Jonkman and M. Buhl, 2005. *FAST User Guide*. National Renewable Energy Laboratory.

[10] ECN, MARIN, L. t. W. T. T. M., 2002. Study to feasibility of and boundary conditions for floating offshore wind turbines. Tech. rep.

[11] M.S., L.-H., D.E., C., and N.D., S., 1961. "Observations of the directionnal spectrum of sea waves using the motions of a floating buoy". *Ocean Wave Spectrum*, pp. 111–136.

[12] Goda, Y., 2010. *Random seas and design of maritime structures*, Vol. 33. World Scientific Pub Co Inc.

[13] Kat, J. D., and Paulling, J., 1989. "The simulation of ship motions and capsizing in severe sea state". Vol. 97, Trans SNMAE, pp. 139–168.

[14] Gilloteaux, J., Babarit, A., Ducrozet, G., Durand, M., and Clment, A., 2007. "A non-linear potential model to predict large-amplitude-motions: Application to the searev wave energy converter". International Conference on Ocean, Offshore and Arctic Engineering.

[15] Morison, J., O'Brien, M., Johnson, J., and Schaaf, S., 1950. "The force exerted by surface waves on piles". *Petrol Trans,* ***189***, pp. 149–154.

[16] Jonkman, J., Butterfield, S., Musial, W., and Scott, G., 2009. Definition of a 5-MW Reference Wind Turbine for Offshore System Development. Tech. Rep. NREL/TP-500-39060, National Renewable Energy Laboratory.

[17] Delhommeau, G., 1993. "Seakeeping codes aquadyn and aquaplus". In 19th WEGEMT School Numerical Simulation of Hydrodynamics: Ships and Offshore Structures.

[18] Cermelli, C. A., and Roddier, D. G., 2005. "Experimental and numerical investigation of the stabilizing effects of a water-entrapment plate on a deepwater minimal floating platform". International Conference on Ocean, Offshore and Arctic Engineering.

[19] Ishihara, T., Waris, M., and Sukegawa, H., 2009. "A study on influence of heave plate on dynamic response of floating offshore wind turbine system". In Proceedings of 3rd European Offshore Wind Conference and Exhibition, Stockholm, Sweden, pp. 14–16.

[20] Bearman, P., Downie, M., Graham, J., and Obasaju, E., 1985. "Forces on cylinders in viscous oscillatory flow at low keulegan-carpenter numbers". *Journal of Fluid Mechanics,* ***154***(1), pp. 337–356.

[21] Sarpkaya, T., and Isaacson, M., 1981. *Mechanics of wave forces on offshore structures*. Van Nostrand Reinhold New York.

[22] Tao, L., and Cai, S., 2004. "Heave motion suppression of a sapr with a heave plate". *Ocean Engineering,* ***31***, pp. 669–692.

[23] Orcina, 2010. *OrcaFlex User Manual v 9.4a*. Orcina Ltd.